A Perturbative Approach to Vibrational Predissociation Rates: Application to ArHF†

ARTICLE *in* THE JOURNAL OF PHYSICAL CHEMISTRY B · JULY 2002

Impact Factor: 3.3 · DOI: 10.1021/jp020397o

3 AUTHORS:

Emmanuel Tannenbaum
Ben-Gurion University of the Negev
51 PUBLICATIONS **312** CITATIONS
SEE PROFILE

Kelly J. Higgins
Harvard University
23 PUBLICATIONS **469** CITATIONS
SEE PROFILE

William Klemperer
Harvard University
99 PUBLICATIONS **4,133** CITATIONS
SEE PROFILE

A Perturbative Approach to Vibrational Predissociation Rates: Application to ArHF†

Emmanuel Tannenbaum, Kelly J. Higgins, and William Klemperer

Department of Chemistry and Chemical Biology, Harvard University, Cambridge, Massachusetts 02138

Bilha Segev

Department of Chemistry, Ben-Gurion University of the Negev, Beer-Sheba 84105, Israel

Eric J. Heller*

Departments of Chemistry and Physics, Harvard University, Cambridge, Massachusetts 02138

Received: February 11, 2002; In Final Form: June 6, 2002

This paper presents a perturbative model for the vibrational predissociation dynamics of inert gas hydrogen halide (RgHX) complexes. The predissociation is modeled as a Fermi Golden Rule (FGR) process from a bound state residing on a two-dimensional potential energy surface (PES) obtained by averaging over the HX vibrational state of interest to a series of one-dimensional exit channels obtained by averaging over the HX rovibrational state of interest. This model is applied to ArHF, for which a high-quality ab initio interaction potential is available. In particular, we focus on the $v \rightarrow v - 1$ transition for the bound states (1000), (2000), (2110), (3000), and (3110). We confirm the experimental observation that the product HF tends to come off at the highest accessible j state, which is $j = 13$ for this system. This results from a strong angular anisotropy in the ArHF interaction potential that couples low-j and high-j HF states. The basic mechanism for this high-j preference is determined to be the suppression of the low-j exit channels arising from highly oscillatory low-j outgoing wave functions. We also observed that the tails of the bound-state wave functions, in the inner wall region of the interaction potential, gave the main contribution to the predissociation rate, indicating that the vibrational predissociation process is due to tunneling and is therefore a purely quantum effect. The calculations also confirm the strong v-dependence of the predissociation rates, as well as the stabilization of the complex that occurs when energy is placed into the HF bending mode. For the (1000) and (2110) states, we obtain rates well below 1600 s^{-1}, which is consistent with the observation by Miller that the vibrational predissociation rates are too slow to be measured. The (2000) state does give a measurable rate, with a computed decay into the $j = 13$ exit channel of 14 000 s^{-1}. The (3000) state gives a corresponding rate of 200 000 s^{-1}, in good agreement with the overall dissociation rate of 250 000 s^{-1}. The (3110) rate is slower, with a value of 12 000 s^{-1}. Though this rate seems somewhat small, given that the lifetime of the (3110) state was measured to only be twice as long as that of the (3000) state, this rate and all our rates are within an order of magnitude of the measured rates.

1. Introduction

The study of the vibrational predissociation of van der Waals and hydrogen-bonded complexes has been an active field of experimental and theoretical research for the past twenty five years. Vibrational predissociation, as a mechanism for converting vibrational energy into translational and rotational energy, may play an important role in relaxation dynamics in gases and liquids, so a proper understanding of it is important.

Some of the most extensively studied complexes are the inert gas hydrogen halide complexes (RgHX). These are the simplest complexes that can have both vibration to rotation and vibration to translation energy transfer. Furthermore, the hydrogen halide complexes have the interesting property that they tend to predissociate with the maximum allowable rotational energy. This is due to the relatively large rotational constants of the HX diatomics, in contrast to the RgX_2 complexes, which tend to predissociate with high translational energy.[1] This pattern is a classic example of the Ewing momentum gap law,[2] which basically states that energy in some initial donor state is transferred preferentially to the final acceptor state (or states) with the least nodal character. This makes sense because highly oscillatory wave functions tend to have little coupling with the initial state. An equivalent formulation of this principle is that energy flows into the state that minimizes the momentum transfer. The HX diatomics have relatively large rotational energy gaps, so minimizing the nodal character of the outgoing waves means placing the excess energy into rotation. The X_2 diatomics have much smaller rotational energy gaps, so minimizing the nodal character of the outgoing waves means placing the excess energy into translation.

Another feature of the RgHX complexes is that their predissociation rates are particularly slow,[3,4] making it difficult to accurately compute their rates. In an early theoretical study, Hutson[5] attempted to calculate the vibrational predissociation rates of ArHCl for $v_{HCl} = 1$ bound states, but his results disagreed with experiment by at least 2 orders of magnitude.[6] In another early study, Halberstadt[7] modeled the $(HF)_2$ dimer

† Part of the special issue "John C. Tully Festschrift".

10.1021/jp020397o CCC: $22.00
Published on Web 07/09/2002

as an RgHF complex to calculate the predissociation rates. However, it is known that complexes with higher degrees of freedom, such as Ar_3HF, $(HF)_2$, and N_2HF, have predissociation rates that are typically several orders of magnitude faster than the RgHF complexes,[4] so it is not clear that modeling $(HF)_2$ as an RgHF complex is accurate.

One of the most commonly studied RgHX complexes is ArHF. ArHF bound states have been studied up to[8] $v_{HF} = 4$, whereas predissociation rates have been studied for[3,9,10] $v_{HF} = 1-3$. The predissociation rates show a strong dependence on v_{HF}. Furthermore, the bound states of ArHF are significantly stabilized when energy is placed into the HF bending mode. The $v_{HF} = 1$ rates were too slow ($<1600\ s^{-1}$) to be observed in measurements by Miller.[9] Some of the $v_{HF} = 2$ rates were measurable,[10] though the rates were still too slow for a value to be assigned. For $v_{HF} = 3$ the rates are sufficiently high to calculate a rotational distribution for the predissociation.[3]

The first attempt to model the predissociation of ArHF via a completely ab initio model was done in ref 1 by Buchachenko, Stepanov, Grigorenko, and Nemukhin. Buchachenko et al. model the predissociation process using a semiempirical ArHF PES obtained using the diatomics-in-molecule approach. Though their approach confirmed the propensity of the HF to come off rotationally hot upon predissociation, and the stabilization of the bound states when energy is placed into HF bending, other features of the model did not agree well with experiment. First of all, experimentally it has been observed that the rotational distribution of product HF decays more or less exponentially from the highest accessible j state, which is $j = 13$ for our system, whereas ref 1 predicted a bimodal distribution. Second, the computed lifetimes were generally an order of magnitude too low. Finally, the lowest energy bound state for $v = 3$ of ArHF is predicted to have a highest accessible exit channel corresponding to $j = 12$. Thus, ref 1 predicts a sudden, significant drop in the predissociation rate from $v = 2$ to $v = 3$, resulting from the closing of the $j = 13$ channel. Experimentally, $j = 13$ is known to remain open all the way through $v = 4$.

Despite their deficiencies, the recent work by Buchachenko et al., and the early work by Hutson and Halberstadt (and others, see references) are all important, because they illustrate the difficulty in computing the rates of the RgHX complexes. The slowness of the rates makes it necessary to use a relatively high-quality ab initio potential, to obtain reasonable agreement with experiment. This was simply not available at the time to Hutson, Halberstadt, or even to Buchachenko et al. Hutson has since developed an accurate empirical potential for ArHF[11] (the H6 (4,3,2) potential), which is essentially a series of two-dimensional, v_{HF}-dependent potentials.

One of us (K.G.H.), generated a high-quality ab initio potential for ArHF using the CCSD(T) method and basis sets developed by Dunning and co-workers[12-14] (a more detailed discussion can be found in ref 15). This potential energy surface (PES) is not averaged over the vibrational states of HF but is rather a three-dimensional potential given in terms of the standard Jacobi coordinates of ArHF. The purpose of this study is to develop a model for the predissociation of RgHX complexes that, in conjunction with the ab initio ArHF potential provided by K.G.H, can qualitatively and quantitatively predict a number of key features of the ArHF predissociation.

The predissociation is modeled as a Fermi Golden Rule (FGR) process from a bound state residing on a PES with the ArHF van der Waals stretch and HF rotation as the slow variables, to outgoing product states residing on PES's with the ArHF stretch as the only slow variable. This approach involves a diabatic separation of the fast HF vibration from the other coordinates of the ArHF complex. The rates are sufficiently slow so as to be indicative of a relatively weak interaction potential. Thus, a perturbative scheme, i.e., FGR, should be the proper approach to this problem. It should be emphasized here that this model is not restricted to ArHF, but rather any RgHX complex for which a three-dimensional PES is available.

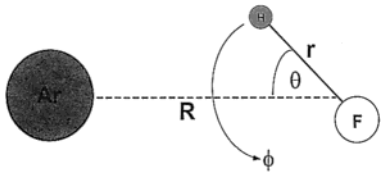

Figure 1. Diagram of the standard Jacobi coordinates of the ArHF geometry, illustrating the four paramters R, r, θ, and ϕ used to characterize the configuration of the system.

This paper is organized as follows: In section 2 we describe in detail our quantum model for the predissociation dynamics of ArHF. In section 3 we present the results and discussion. We analyze the results obtained, comparing them with what is known experimentally, and also address some numerical issues involved in computing the predissociation rates. Finally, we conclude in section 4 with a summary of our main results and discuss future research.

2. The Model

All calculations were done in a dimensionless system of units with a reference mass of 1 amu, a reference length of 1 Å, and a reference wavenumber of 1000 cm^{-1}. Subsection 2.1 presents the Hamiltonian governing the dynamics of the ArHF complex. Subsection 2.2 presents the diabatic approach used to compute the bound states of interest in this paper. Subsection 2.3 presents the method to determine the outgoing states. Subsection 2.4 gives the FGR formula for the predissociation rates into the various exit channels. Finally, subsection 2.5 presents a semi-analytic approach to evaluate the FGR formula using the Wigner transform. The purpose of this approach is to supplement the direct calculations, to circumvent numerical difficulties associated with extracting slow rates from highly oscillatory integrals.

2.1. The Hamiltonian. A diagram of the standard Jacobi coordinates of ArHF is given in Figure 1. We define μ to denote a reduced mass and set $\mu_r = \mu_{HF}$ and $\mu_R = \mu_{ArHF}$. We shall neglect the Coriolis coupling terms, so that we can work in a body-fixed coordinate axis. Finally, by multiplying our wave functions by Rr, where $R \equiv |\vec{R}|$, $r \equiv |\vec{r}|$, our Hamiltonian becomes

$$\hat{H} = \frac{\hat{p}_R^{\,2}}{2\mu_R} + \frac{\hat{p}_r^{\,2}}{2\mu_r} + u(r) - \frac{\hbar^2}{2\mu_r r^2}\left(\frac{1}{\sin\theta}\frac{\partial}{\partial\theta}\left(\sin\theta\frac{\partial}{\partial\theta}\right) + \frac{1}{\sin^2\theta}\frac{\partial^2}{\partial\phi^2}\right) + V(R,r,\theta) \qquad (1)$$

where $u(r)$ denotes the HF interaction potential, and $V(R,r,\theta)$ is the interaction between Ar and HF.

The bound states are characterized as $(vjKn)$, where v is the HF vibrational quantum number, j corresponds to $\mathbf{J}^2$ for HF in the limit of infinite ArHF bond distance, K corresponds to $j_z \equiv -i\hbar\partial/\partial\phi$, and n is the vibrational quantum number for the Ar$\cdot\cdot\cdot$HF stretch. Note that because j_z commutes with the ArHF Hamiltonian, we need only worry about couplings among

identical K states. Thus, all calculations in this paper are carried out at constant K, which is dictated by the bound state of interest.

The ab initio potential, $V(R,r,\theta)$, was generated on a grid with $R = 2.5, 2.7, 2.9, 3.1, 3.3, 3.5, 3.7, 3.9, 4.1, 4.3, 4.5, 5.0, 5.5, 6.0, 6.5, 7.0, 8.0, 9.0, 10.0$, $r = 0.6, 0.7159, 0.85, 0.9168, 0.9326, 0.9648, 0.998, 1.0324, 1.063\,57, 1.098\,16, 1.2, 1.318\,07, 1.4, 1.5, 1.6, 1.7$, all in Å, and $\theta = 0-180°$ in 15° intervals. A detailed discussion on the calculation of the free-HF basis and the evaluation of the potential couplings may be found in Appendix A.

2.2. Determining the Bound States. For low rotational quantum numbers j, both R and θ are slow variables with respect to r. Thus, the low-j bound states of ArHF (the only ones we are interested in for this study) reside on a two-dimensional PES obtained by averaging over the vibrational quantum state of interest. To determine the bound states for a given vibrational quantum number v, we proceed as follows: We write the full ArHF Hamiltonian as

$$\hat{H} = \frac{\hat{p}_R^{\,2}}{2\mu_R} + \hat{H}_{HF}(r,\theta) + \hat{V}(R,r,\theta) \qquad (2)$$

The eigenstates are expanded in the product basis $|n\rangle|v,j,K\rangle$, where $|v,j,K\rangle$ denote the free-HF wave functions and $|n\rangle$ denotes the particle-in-a-box states for $R \in [L_1, L_2]$, where $[L_1, L_2]$ is a user-specified interval. The energies of these states are $E_n = \hbar^2\pi^2n^2/2\mu_R L^2$, where $L \equiv L_2 - L_1$. This is admittedly an unusual choice of basis. However, because our potential data are only given over a limited range, we wanted to be able to force the bound states to vanish outside this range to make the numerical integrations exact. The tails of the bound states are sufficiently small outside the range of potential data for which this is a valid assumption.

As discussed previously, for a given calculation we work at constant K, so the matrix elements are then given by

$$\langle n'|\langle v',j',K|\hat{H}|v,j,K\rangle|n\rangle = (E_n + E_{vj})\delta_{nn'}\delta_{vv'}\delta_{jj'} + \langle n'|\langle v',j',K|\hat{V}(R,r,\theta)|v,j,K\rangle|n\rangle \qquad (3)$$

For the bound state lying on the PES corresponding to a given vibrational quantum number v, we take $v' = v$, and so the matrix elements on this PES are given by $(E_n + E_{vj})\delta_{nn'}\delta_{jj'} + \langle n'|\langle v,j',K|\hat{V}(R,r,\theta)|v,j,K\rangle|n\rangle$. The couplings $\langle n'|\langle v,j',K|\hat{V}(R,r,\theta)|v,j,K\rangle|n\rangle$ are evaluated numerically by using a linear interpolation to $\langle v,j',K|\hat{V}(R,r,\theta)|v,j,K\rangle$ in R.

We then diagonalize the Hamiltonian in this basis to obtain the bound states within the fixed-v subspace. A given bound state is expressible as $\Sigma_{n,j}c_{nj}|n\rangle|v,j,K\rangle = \Sigma_j\Sigma_n c_{nj}|n\rangle|v,j,K\rangle$. Now, $\Sigma_{n,j}c_{nj}|n\rangle$ describes a wave function $\psi_j(R)$, so that our bound state may be written as $\Sigma_j\psi_j(R)|v,j,K\rangle$.

This method is not the standard Born−Oppenheimer approach for finding the bound states when R and θ are slow variables compared to r. Rather, we make a diabatic separation of the fast HF vibration coordinate r from the slow variables R and θ. The geometry of the problem is well-suited to such an approach. The reason for this is that the ArHF binding energy of 100 cm^{-1} is small compared to the HF vibrational energy spacing of 3000 cm^{-1}. Thus, the ArHF interaction only weakly distorts the fast HF vibration.

For the R coordinate particle-in-a-box states, we used two sets of box dimensions and basis set sizes for the bound-state calculations. In the first set, we made the dimensions and basis set size as small as possible without affecting the energy of the desired bound state. This was done so as to eliminate any residual small oscillations at the wave function tails. In the second set, we used larger box dimensions but used the smallest basis set possible to get the same energies as in the first set. Though the two sets of bound states appear identical, residual oscillations at the tails of the second set could lead to different dissociation rates. We computed the dissociation rates using both sets of bound states, to determine the numerical stability of the final answers.

TABLE 1: Energies of a Sample of ArHF Bound States (cm^{-1}) with Respect to the Corresponding $v, j = 0$ Free-HF State[a]

state	ab initio	experiment	L^1_{min}	L^1_{max}	N_1			$L^2_{min}L^2_{max}N_2$
(1000)	−99.99	−111.35	2.8	4.6	25	2.6	6.0	35
(2000)	−108.66	−122.61	2.8	4.7	25	2.6	6.0	40
(2110)	−38.06	−46.35	2.8	4.8	25	2.6	6.0	30
(3000)	−118.84	−135.47	2.9	4.5	20	2.6	6.0	30
(3110)	−42.86	−52.13	2.8	4.7	10	2.6	6.0	15

[a] Column 2: The calculated energies. Column 3: The experimental energies. Columns 4 and 5: The first set of box dimensions. Column 6: The maximum particle-in-a-box energy level in the basis used for the first set of box dimensions ($n = 1 - N_{max}$). Columns 7 and 8: The second set of box dimensions. Column 9: The maximum particle-in-a-box energy level in the basis used for the second set of box dimensions.

In Table 1 we present the calculated energies for the (1000), (2000), (2110), (3000), and (3110) bound states. These are the bound states whose predissociation rates we consider in this paper. We also present the experimentally measured energies, which are also given in ref 15. In addition, we give the box dimensions and basis set size used to obtain these energies. Note that convergence is fairly rapid, requiring no more than 40 basis states. This is to be expected, because the ArHF interaction is fairly weak (as compared with the HF potential).

The agreement between theory and experiment is fairly good; however, as with the free-HF states, we use the experimental values for the energies in the dissociation calculations in this paper. The reasons for this are discussed in the Conclusions and in Appendix A.1 on the free-HF basis.

2.3. Determining the Outgoing States. To determine the dissociated wave function corresponding to product HF exiting with energy E in the state $|v,j,K\rangle$, we average the Hamiltonian over the state $|v,j,K\rangle$ of interest, thereby obtaining a PES depending only on R, on which we can construct the outgoing wave. For the high-j states, the rotational energy gaps are on the order of 500 cm^{-1}, whereas the translational energy gaps are on the order of a few tens of cm^{-1}. Thus, at high-j, both r and θ are fast variables, so that this approach is exactly the crude Born−Oppenheimer approximation. We expect negligible mixing among the high-j channels, so that the decay rates into them are equivalent to the decay rates into the corresponding product HF states. For the lower j states, only r is a fast variable, so that this approach neglects mixing among the low-j channels. Thus, though the couplings to these channels are sufficiently small so that the decay rates into them are given by an FGR approach, interchannel mixing makes these decay rates different from the decay rates into the corresponding product HF states. Nevertheless, because we expect the product HF to be rotationally hot, the decay rates into the low-j channels should be negligible, rendering interchannel mixing irrelevant. Thus, this method is directly applicable only to the RgHX complexes. For the RgX_2 complexes the decay rates are predominantly into the low-j channels, so channel mixing needs to be taken into account to properly determine the rotational distribution.

The determination of the outgoing wave functions is detailed in Appendix A.3.

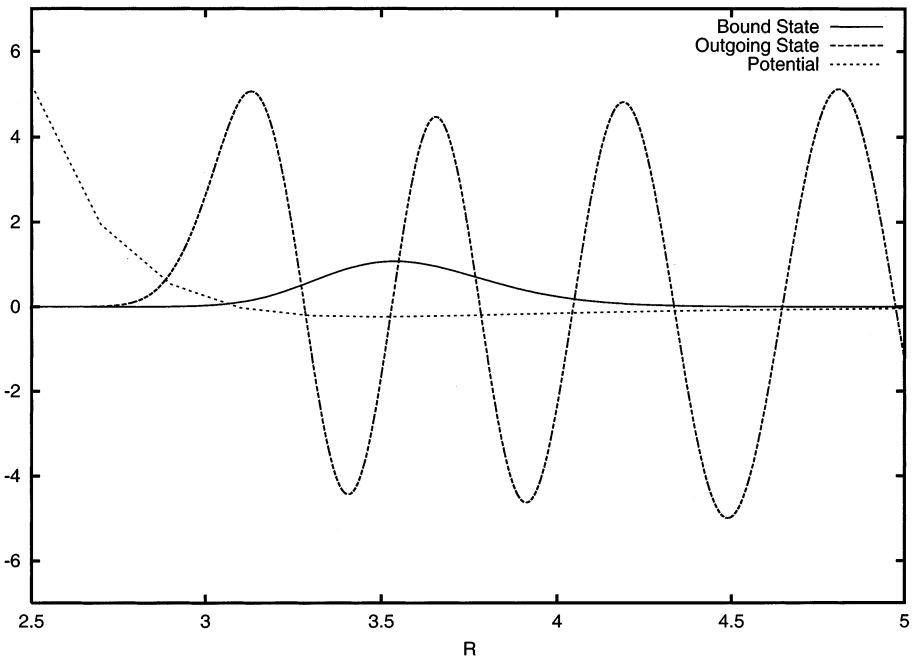

Figure 2. Qualitative illustration of the coupling between a bound state and a given exit channel. The plot is of some $\psi_j(R)$ component of a given bound state, some outgoing wave $\phi_{j'}(R)$, and the coupling $V_{(v-1)vj'j}(R)$.

2.4. Computing the Dissociation Rate. The dissociation rate is computed using Fermi's Golden Rule. For a bound-free dissociation process in which the outgoing continuum states have the $\delta(E - E')$ normalization, the FGR formula gives a decay rate into a given exit channel of

$$\Gamma = \frac{2\pi}{\hbar}|\langle\phi_o|\hat{H}|\phi_b\rangle|^2 \tag{4}$$

where $|\phi_b\rangle$ denotes the bound state and $|\phi_o\rangle$ denotes the given exit channel outgoing state with energy equal to the bound-state energy. The key feature to note here is that the predissociation is from a bound state obtained from a Hamiltonian with two slow variables, to outgoing states obtained from a Hamiltonian with one slow variable. Nevertheless, the FGR rate is obtained by inserting the full Hamiltonian $\hat{H}$ between the bound state and a given outgoing state. The basic idea is that although the bound and outgoing states are generated from different Hamiltonians, they lie on surfaces with different free-HF vibrational quantum numbers, and so the only term in the Hamiltonian that couples the bound and outgoing states is the ArHF interaction $V(R,r,\theta)$.

The bound state is given by $\Sigma_j\psi_j(R)|v,j,K\rangle$, and because we look at $v \rightarrow v-1$ transitions, the outgoing state is given by $\phi_{j'}(R)|v-1,j',K\rangle$. The coupling integral is evaluated numerically. A qualitative illustration of the coupling between a bound state and a given exit channel is given in Figure 2.

2.5. Semianalytical Model. As we shall see in the Results and Discussion, the highly oscillatory outgoing wave functions make it difficult to accurately compute the lower j predissociation rates. The result of this is that the numerics prevent us from extracting the rotational distribution predicted by the model. It would be desirable to supplement our calculations with another integration technique that more faithfully reproduces the rotational distribution. To this end, we begin by defining $|\psi_{vj'}\rangle$ via $\langle R|\psi_{vj'}\rangle = \psi_{vj'}(R) = \Sigma_j\psi_j(R)V_{(v-1)vj'j}(R)$, where $V_{(v-1)vj'j}(R) \equiv \langle v-1,j',K|\hat{V}|v,j,K\rangle$. Then

$$\langle\phi_o|\hat{H}|\phi_b\rangle = \int_{-\infty}^{\infty}dR\phi_{j'}(R)\,\psi_{vj'}(R) = \langle\phi_{j'}|\psi_{vj'}\rangle \tag{5}$$

where $\phi_{j'}(R) = \psi_{vj'}(R) = 0$ for $R \in \mathbf{R}/[R_{min}, R_{max}]$. The FGR rate into the $|v-1,j',K\rangle$ channel is then given by $2\pi/\hbar|\langle\phi_{j'}|\psi_{vj'}\rangle|^2$. We can eliminate the oscillatory nature of the overlap integral by applying the Wigner transform to both $\psi_{vj'}(R)$ and $\phi_{j'}(R)$. Briefly, the Wigner transform converts a wave function $\psi(R)$ into a two-dimensional phase-space distribution function $\rho_{W,\psi}(R, p_R)$. It is given by

$$\rho_{W,\psi}(R,p_R) = \frac{1}{2\pi\hbar}\int_{-\infty}^{\infty}ds\;\psi(R+s)\;\bar{\psi}(R-s)\exp(-2ip_Rs/\hbar) \tag{6}$$

The FGR rate may then be written as

$$\Gamma = 16\pi^2\int_{-\infty}^{\infty}\int_{-\infty}^{\infty}dR\;dp_R\;\rho_{W,\psi_{vj'}}(R,p_R)\;\rho_{W,\phi_{j'}}(R,p_R) \tag{7}$$

At first glance, it may appear that we have simply complicated the problem by introducing two integration variables, instead of just one. However, because $\phi_{j'}(R)$ is the eigenstate of energy E of the one-dimensional Hamiltonian

$$H_{vj'}(R,p_R) = \frac{{p_R}^2}{2\mu_R} + V_{vj'}(R) + E_{vj} \tag{8}$$

where $V_{vj'}(R) \equiv \langle v,j',K|\hat{V}|v,j',K\rangle$, to lowest order in it can be shown that $\rho_{W,\phi j'}(R,p_R) = (1/4\pi\hbar)\delta(E-H_{vj'}(R,p_R))$; that is, $\rho_{W,\phi j'}$ is simply proportional to the classical microcanonical distribution. Thus, the oscillatory nature of the overlap integral has been eliminated. Furthermore, the initial state distribution $\psi_{vj'}(R)$ may be reasonably approximated with a Gaussian, so that its Wigner transform is itself a Gaussian. This results in an integral that can be readily evaluated using MATHEMATICA. Of course, working only to lowest order in $\hbar$ will lead to discrepancies between the direct integrations and our semianalytic results. Nevertheless, this semiclassical approximation may be systematically improved, and future research would involve bringing this Wigner-based approach into quantitative agreement with the direct integrations.

TABLE 2: Dissociation Rates for the (1000) State[a]

product state	decay rate 1 (s^{-1})	decay rate 2 (s^{-1})
$\|0, 13\rangle$	1.67×10^2	1.67×10^2
$\|0, 12\rangle$	8.95×10^0	1.13×10^1
$\|0, 11\rangle$	1.66×10^0	1.59×10^0
$\|0, 10\rangle$	1.04×10^1	1.14×10^1
$\|0, 9\rangle$	8.01×10^2	4.01×10^2

[a] Column 1 gives the rates corresponding to the bound state computed using the first set of box dimensions. Column 2 gives the rates corresponding to the bound state computed using the second set of box dimensions.

TABLE 3: Dissociation Rates for the (2000) State[a]

product state	decay rate 1 (s^{-1})	decay rate 2 (s^{-1})
$\|1, 13\rangle$	1.39×10^4	1.39×10^4
$\|1, 12\rangle$	8.06×10^1	7.17×10^1
$\|1, 11\rangle$	1.34×10^3	1.29×10^3
$\|1, 10\rangle$	3.00×10^3	2.56×10^3
$\|1, 9\rangle$	1.11×10^2	4.72×10^1

[a] Column 1 gives the rates corresponding to the bound state computed using the first set of box dimensions. Column 2 gives the rates corresponding to the bound state computed using the second set of box dimensions.

TABLE 4: Dissociation Rates for the (2110) State[a]

product state	decay rate 1 (s^{-1})	decay rate 2 (s^{-1})
$\|1, 13\rangle$	6.24×10^1	6.31×10^1
$\|1, 12\rangle$	7.05×10^1	9.35×10^1
$\|1, 11\rangle$	7.83×10^2	6.07×10^2
$\|1, 10\rangle$	3.42×10^1	9.38×10^0
$\|1, 9\rangle$	5.65×10^2	3.98×10^2

[a] Column 1 gives the rates corresponding to the bound state computed using the first set of box dimensions. Column 2 gives the rates corresponding to the bound state computed using the second set of box dimensions.

TABLE 5: Dissociation Rates for the (3000) State[a]

product state	decay rate 1 (s^{-1})	decay rate 2 (s^{-1})
$\|2, 13\rangle$	1.99×10^5	1.98×10^5
$\|2, 12\rangle$	4.31×10^3	3.82×10^3
$\|2, 11\rangle$	2.54×10^3	4.24×10^3
$\|2, 10\rangle$	2.16×10^4	1.72×10^4
$\|2, 9\rangle$	2.54×10^4	1.56×10^4

[a] Column 1 gives the rates corresponding to the bound state computed using the first set of box dimensions. Column 2 gives the rates corresponding to the bound state computed using the second set of box dimensions.

The above approach to this particular system was developed in ref 16.[17] This reference also contains a good review of the Wigner transform formalism.

3. Results and Discussion

3.1. Dissociation Rates. The FGR predissociation rates were computed for the (1000), (2000), (2110), (3000), and (3110) states. Two sets of rates were computed, corresponding to the two sets of bound states obtained. The results are presented in Tables 2−6.

We begin by noting that only the $j = 13$ rates are relatively stable to variations in the box length L. The rates show significant discrepancies between the two sets of bound states already at $j = 12$. We will discuss the reasons for this later in this section. We should note that our semianalytic model using the Wigner transform deals with this problem quite well. We will also return to this later, but for now we should note that it indicates that the rates drop off sharply with decreasing j, so that essentially all of the dissociation occurs into the $j = 13$ channel. The experimental distribution is considerably broader. Possible reasons for this discrepancy will be discussed. For now, however, we will focus on the $j = 13$ rates for the various bound states, because we believe that these are the only ones that are significant.

TABLE 6: Dissociation Rates for the (3110) State[a]

product state	decay rate 1 (s^{-1})	decay rate 2 (s^{-1})
$\|2, 13\rangle$	1.21×10^4	1.24×10^4
$\|2, 12\rangle$	1.48×10^2	4.72×10^2
$\|2, 11\rangle$	1.83×10^3	1.62×10^2
$\|2, 10\rangle$	3.87×10^3	2.04×10^4
$\|2, 9\rangle$	1.08×10^3	1.14×10^3

[a] Column 1 gives the rates corresponding to the bound state computed using the first set of box dimensions. Column 2 gives the rates corresponding to the bound state computed using the second set of box dimensions.

The predissociation rate from the (1000) state to the $|0, 13\rangle$ exit channel was determined to be ≈ 170 s^{-1}. Using our semianalytic Wigner transform approach, we obtained a corresponding rate of 1570 s^{-1}. Both these rates are below 1600 s^{-1}, which is currently around the lower limit for an experimentally measurable rate. Thus, we have managed to confirm the experimental observation that the (1000) predissociation rate is too slow to be measured.[9] Though future work is necessary to bring the Wigner-based approach into quantitative agreement with the direct integration, both results are nevertheless consistent with experiment.

For the (2000) state, we get a vibrational predissociation rate into the $|1, 13\rangle$ channel of $\approx 14\,000$ s^{-1}, which is measurable. The semianalytic value is $\approx 16\,000$ s^{-1}. Indeed, the (2000) decay rate has been measured by Miller,[10] although an actual number was not given. Therefore, all we can say about the (2000) state at this point is that our numerics are consistent with the fact that this state has a measurable predissociation rate.

For the (2110) state, we get a vibrational predissociation rate into the $|1, 13\rangle$ channel of ≈ 60 s^{-1}, which is much too small to be measured. The semianalytic value is 1070 s^{-1}. Again, though the two rates are off by an order of magnitude, they are both consistent with the rates being too slow to be currently measurable. Indeed, it has been observed experimentally by Miller that the (2110) state predissociates too slowly to have a measurable rate.

We calculated the predissociation rate of the (3000) state into the $|2, 13\rangle$ exit channel to be $\approx 200\,000$ s^{-1}, as compared with the experimentally measured value of 120 000 s^{-1}. The corresponding semianalytic result is 160 000 s^{-1}. Our computed rate is thus well within the order of magnitude of the measured rate.

Finally, the vibrational predissociation rate of the (3110) state into the $|2, 13\rangle$ exit channel was calculated to be $\approx 12\,000$ s^{-1}. The semianalytic value was 7600 s^{-1}. These values, though within an order of magnitude of the measured rate, seem somewhat low, given that the (3110) lifetime is only twice as long as the (3000) lifetime.[3] We do not have an explanation for this discrepancy, because the numerics seem fairly clear cut. One possibility on the computational side has to do with the fact that the wave function tails are the main contributors to the predissociation rates. This tends to make the rates somewhat sensitive to the shape of the bound states. Given that our bound-state energies typically have errors on the order of 10−15%, there could be sufficient errors at the tails to significantly affect the computed rates. Errors in the ab initio potential may further contribute to this discrepancy with experiment. Whereas the ArHF potential is of a high quality, the largest errors lie in the

inner wall (small R) region of the potential, where the electrostatic interactions are greatest. Because this coincides with the location of the bound-state tails, the result is a further enhancement of the error associated with computing the predissociation rates.[3]

Two features of interest are the strong v dependence of the predissociation rates, and the stabilizing effect that occurs when j and K are increased from 0 to 1. The first feature can be explained by noting that as v is increased, the average HF bond length increases, and so the HF experiences a stronger interaction with Ar. The result is an increased coupling to the outgoing states, and consequently a faster predissociation rate. The effect is dramatic: The (3000) predissociation rate is 2−3 orders of magnitude larger than the (1000) predissociation rate (depending on whether one uses the exact or semianalytic (1000) result). Indeed, Klemperer and co-workers have argued that a v^4 power law describes the pattern of the (v000) predissociation rates.[3]

The second feature can be explained by noting that increasing j, K from 0 to 1 gives HF some rotational energy and places some of the HF rotation into the plane perpendicular to the ArHF van der Waals vector $\vec{R}$. This reduces the extent to which the HF samples the anisotropy of the ArHF interaction inside the potential well. This also results in the $K = 1$ bound states being more weakly bound than the $K = 0$ bound states, leading to a larger energy gap between the bound states and the outgoing channels. Therefore, their lifetimes are considerably longer. This accounts for the (2000) predissociation rate being measurable, but the computed rate for (2110) being too slow to be measurable. As noted above, our calculations may be overestimating this effect, because the computed predissociation rate of the (3000) state is approximately 20 times larger than that of the (3110) state.

3.2. The Rotational Distribution. As mentioned previously, we encountered numerical difficulties computing the predissociation rates already for $j = 12$. This will be addressed shortly, but for now we should note that the semianalytic approach based on the Wigner transform did not encounter any such numerical difficulties. To get an idea of what our computed rotational distribution should look like, we computed the predissociation rates for the (3000) bound state into the $|v = 2, j = 12, 11, 10, 9, K = 0\rangle$ exit channels. The semianalytic results are 0.0015 and 0.00019 s^{-1}, respectively. A similar pattern was obtained with the other states, which persists all the way down to the low-j channels. Given that the semianalytic approach quantitatively reproduces the $j = 13$ rates, we believe that this is strong evidence that numerically essentially all of the predissociation occurs into the $j = 13$ channel, and that there is a sharp, continuous decay in the predissociation rates with decreasing j.

In any event, our model successfully captures the experimental observation that the ArHF complex preferentially predissociates into the highest accessible rotational channel. The main discrepancy with experiment is that our rotational distribution is considerably sharper than that observed experimentally. One possible source of this discrepancy is our neglect of interchannel coupling at high-j. Thus, it could be that the $j = 13$ channel serves as a gateway for FGR decay into the lower j channels. To check this, we computed the interchannel couplings for the various bound states. Because we are dealing with $\delta(E - E')$ normalization in the outgoing channels, the interchannel couplings are dimensionless. To use a specific case, for the (3000) state the $j = 13/j = 12$ coupling was ≈0.006. Because the relevant parameter for FGR is $|\hat{V}|^2$ as opposed to $|\hat{V}|$, we get that the rate into the $j = 12$ channel should be on the order of $0.006^2 \times 200\,000\ s^{-1} = 7.2\ s^{-1}$, where 200 000 s^{-1} is the rate into the $j = 13$ channel. As a comparison, the $j = 1/j = 0$ coupling was ≈0.17. This gives a $|\hat{V}|^2$ that is 800 times larger than that for the $j = 13/j = 12$ coupling. A similar pattern was observed for the other states, so we obtain that interchannel coupling appears to give a negligible contribution to the rates at high-j. At low-j interchannel coupling becomes significant but is unimportant because the low-j predissociation rates are negligible.

The interplay of three factors results in a rotationally hot product HF. First of all, the more excess vibrational energy is placed into translation, the more oscillatory the corresponding outgoing wave. This results in a suppression of the predissociation rates as one goes from high-j to low-j. Of course, placing energy into rotation results in an oscillatory angular component to the outgoing wave function. This would have a tendency to suppress the high-j rates relative to the low-j rates. However, the lightness of H gives HF a relatively large rotational constant, so that for a given energy, the oscillatory character of the outgoing wave is minimized by placing the energy into rotation. Finally, the ArHF interaction potential has a strong θ anisotropy, which monotonically increases with $|r - r_{eq}|$. Indeed, a plot of V as a function of θ revealed a sharply peaked Gaussian about $\theta = 0°$. This allows for effective coupling between the low-j components of the bound states to the high-j outgoing waves. Though the low-j/low-j couplings are significantly stronger, the anisotropy makes the low-j/high-j couplings sufficiently strong so that, combined with the previous two effects suppressing the low-j channels relative to the high-j ones, a rotationally hot product HF results.

3.3. Numerical Issues. We may note that the two sets of rates given in Tables 2−6 already show significant discrepancies at $j = 12$, in many cases differing by more than an order of magnitude. This can be explained fairly simply: As we go to lower j, the outgoing states have more translational energy, making them more oscillatory. Furthermore, the (r, θ) couplings from the low-j states comprising the bound states to the outgoing states increase by several orders of magnitude as we drop to lower j. The result is that as we go to lower j, the numerical integration involves adding larger and larger numbers of more rapidly varying sign. Though we expect the oscillatory nature of the outgoing waves to essentially kill the coupling at lower j, numerically the cancellation is not perfect. For the higher j states, the integral is less oscillatory, and the couplings are much smaller, so the additions and subtractions do not need to be as exact as for the lower j to get an accurate rate. This explains why no matter what the $j = 13$ rate is for all the bound states, the lowest j rates ($j \approx 0-3$) tend to jump to values on the order of 10^3 to 10^5 s^{-1}. In our dimensionless system of units, this corresponds to a rate on the order of 10^{-11} to 10^{-9}.

In ref 1 Buchachenko et al. obtained a rotational distribution that had a bimodal character. Their calculations gave bound-state lifetimes that were typically an order of magnitude too low. We believe that this bimodal distribution, as well as the low lifetimes, is at least partly due to the numerical issues described here. As can be seen in Tables 2−6, the numerical integrations give a bimodal distribution, and significantly overestimate the low-j rates, so that the total predissociation rates are an order of magnitude or more larger than those measured experimentally.

4. Conclusions and Future Research

This paper developed a model for the vibrational predissociation dynamics of RgHX complexes as an FGR decay from a bound state residing on a two-dimensional PES to a series of

one-dimensional exit channels. Using a high-quality ab initio ArHF PES, we applied this model to the ArHF complex. This model gave rates for the (1000) and (2110) states that were consistent with the observation that predissociation of these bound states is too slow to be currently measured. The computed rate for the (2000) state was found to be consistent with its predissociation being observable, though no actual experimental value has been given to date. For the (3000) state, the computed $j = 13$ predissociation rate of 200 000 s^{-1} is in good agreement with the overall predissociation rate of 250 000 s^{-1}. Indeed, of the five bound states considered in this paper, the only problematic state is the (3110) state, whose computed predissociation rate into the $j = 13$ channel of 12 000 s^{-1} is somewhat low, though still within an order of magnitude of experiment. Numerical tests with a distorted potential suggest that this rate discrepancy may have nothing to do with our theoretical approach to the problem, but rather may be due to errors in the ab initio PES for ArHF, in particular at small R.

Though our approach was not a pure ab initio one, in that we adjusted the free-HF and bound-state energies to the experimentally calculated ones (see Appendix A.1), we should note that a full ab initio approach would nevertheless have given similar results to the ones obtained in this paper. To illustrate, using adjusted free-HF and bound-state energies gave a predissociation rate from the (3000) to the $|v = 2, j = 13, K = 0\rangle$ exit channel of 200 000 s^{-1}, with a product HF translational energy of 87 cm^{-1}. A pure ab initio calculation, with no parameters adjusted, gave a corresponding decay rate of 160 000 s^{-1} and a translational energy of 54 cm^{-1}.

Our model successfully predicts the strong v-dependence of the predissociation rates, as well as the stabilization of the bound states that occur when j, K, are increased from 0 to 1. Combined with the semianalytic results, we also managed to confirm the experimental observation that the product HF tends to come off with the highest accessible j, which was $j = 13$ for the bound states considered. As mentioned in the previous section, this results from the interplay of three factors: (1) The relatively large rotational constant of HF. (2) A strong angular anisotropy in the ArHF interaction potential (the Gaussian in θ mentioned in the previous section). (3) Highly oscillatory low-j outgoing waves, as compared to high-j outgoing waves, which suppress the predissociation rates into the low-j channels as compared to the high-j ones. We should note that this explanation is not original, having been noted, for instance, in ref 1. However, we felt it should be restated here, because it is a conclusion that follows from our investigations. In fact, as discussed in the Introduction, it can be argued that this explanation is actually due to Ewing (up to some details particular to this system).

The main discrepancy between our model and experiment is that our model predicts essentially all of the predissociation to occur into the $j = 13$ channel. The semianalytic computations give a sharp, more or less exponential decay in the rates with decreasing j. Experimentally the distribution is considerably broader, with significant probability in the $j = 9-13$ range. The experimental decay is also essentially exponential, with a slight exception for the (3110) state, which shows a slightly larger $j = 12$ rate than the $j = 13$ rate. Our current numerical evidence suggests that interchannel mixing has a negligible effect on the rotational distribution, so that at this point we do not have a good explanation for these discrepancies. A higher level of theory may be required to properly address this situation, either in the computation of the bound states, or in the outgoing channels, or both. The simplicity of our current model makes it a convenient springboard for more complicated, and hopefully more accurate, approaches. We leave this for future work.

As mentioned previously, it may also be necessary to obtain a more accurate ab initio PES. It should be re-emphasized that the slowness of the predissociation rates make their numerical evaluation difficult. This is especially true for the lower j rates, where their slowness complicates their accurate evaluation due to oscillatory integrals. Thus, although the current ab initio ArHF PES is of relatively high quality, it is not clear that we could have obtained much better results with it using a higher level of theory.

On the experimental side, we should note that one of us (W.K.) has reason to believe that the current measurements on the $v = 3$ bound states of ArHF may overestimate the lower j populations. This is therefore an issue that may also require further experimental investigation. It could very well happen that the true rotational distributions fall somewhere between the current theoretical and experimental results.

We should also restate here that the main contribution to the bound-free coupling is in the inner wall region of the ArHF potential, at the bound-state tails. This means that the bulk of the bound-free coupling is in the classically forbidden region, so that the predissociation process is due to tunneling and is therefore a purely quantum effect. Classical simulations will fail to take the inner wall region of the ArHF potential into account and so will give predissociation rates that are too low.

Our current model can be used to study other RgHX complexes, provided that an ab initio potential can be obtained for those. In particular, one complex of interest is KrHF, whose predissociation even at $v_{HF} = 3$ is too slow to be measured. One possible explanation for this is that the KrHF interaction potential is signficantly stronger than the ArHF interaction. This could result in a bound-state energy sufficiently low to close the $j = 13$ channel, leading to a sharp drop in the predissociation rates.

Future research plans involve extending our model to study other van der Waals complexes, such as CO−HF, N_2HF, $(HF)_2$, and Ar_3HF. These complexes have predissociation rates that are several orders of magnitude larger than those of ArHF, and it would be interesting to see if this can be confirmed numerically. Although these systems are computationally more difficult to work with because they have more degrees of freedom, it may be possible to more accurately extract the predissociation rates because they are much larger. Finally, we hope to develop the Wigner approach and see if it is possible to bring it into quantitative agreement with the numerics for all the bound states considered. Because the Wigner-based approach does not suffer from the same numerical instabilities that direct integration does, such an approach could replace the direct integration as a method for computing the predissociation rates. The Wigner-based approach has the additional advantage that it provides physical insight, by giving a phase-space picture of the predissociation process.

Acknowledgment. This research was supported by the Department of Chemistry and Chemical Biology at Harvard, the Department of Physics at Harvard, by an NSF Graduate Research Fellowship, and by Grant No. 2000118 from the United States−Israel Binational Science Foundation (BSF), Jerusalem, Israel.

A. Numerical Details

In this Appendix, we present some numerical details of the calculations in this paper. These calculations were not regarded

as sufficiently interesting to be included in the main body of the paper. They are included here to aid interested researchers in reproducing our results and possibly refining and extending the predissociation model.

A.1. The Free-HF Basis. The rovibrational states of HF were obtained by assuming a Morse interaction potential, with a ground-state harmonic frequency $\omega = 4138.32\ \mathrm{cm}^{-1}$, and a dissociation energy of $D = 47\,628\ \mathrm{cm}^{-1}$. We obtained our free-HF eigenfunctions for $v = 0-4$ and $j = 0-14$. The equilibrium bond length r_{eq} of HF is also known and is equal to 0.9168 Å. The actual free-HF energies differ slightly from those obtained using the Morse potential approximation. An excellent fit, accurate to within 1 cm^{-1}, is given by the Dunham expression,[17]

$$E_{vj} = \left(Y_{10}\left(v+\frac{1}{2}\right) + Y_{20}\left(v+\frac{1}{2}\right)^2 + Y_{30}\left(v+\frac{1}{2}\right)^3\right) + \left(Y_{01} + Y_{11}\left(v+\frac{1}{2}\right) + Y_{21}\left(v+\frac{1}{2}\right)^2\right)j(j+1) + \left(Y_{02} + Y_{12}\left(v+\frac{1}{2}\right) + Y_{22}\left(v+\frac{1}{2}\right)^2\right)(j(j+1))^2 \quad \text{(A1)}$$

where $Y_{10} = 4138.32$, $Y_{20} = -89.88$, $Y_{30} = 0.90$, $Y_{01} = 20.9557$, $Y_{11} = -0.798$, $Y_{21} = 0.0127$, $Y_{02} = 0.002151$, $Y_{12} = -6.8 \times 10^{-5}$, $Y_{22} = 2.8 \times 10^{-6}$, all in units of cm^{-1}.

Because the corrections to the free-HF energies computed with the Morse potential are small (at most a few percent), we decided that the free-HF eigenfunctions computed from the Morse potential were sufficiently accurate for the calculations in this paper. However, because a highly accurate expression for the free-HF spectrum is available, we decided to use it to compute the free-HF energies once our Morse potential calculations converged.

A.2. Potential Couplings. To determine the representation at a given R of $V(R,r,\theta)$ in the free-HF basis, we start by writing the free-HF states $|v,j,K\rangle$ as $\Sigma_k c_{vk}|k\rangle|\ j,K\rangle$, where $\{|k\rangle\}$ are the harmonic-oscillator eigenfunctions corresponding to the ground-state harmonic frequency of the Morse potential. Then the coupling $\langle v',j',K|\hat{V}|v,j,K\rangle$ is given by $\Sigma_{k,k'} c_{v'k'} c_{vk} \langle j',K|\langle k'|\hat{V}|k\rangle|j,K\rangle$. This proved to be a convenient way to compute the couplings, because harmonic-oscillator eigenstates are relatively easy to handle.

We converted from the r representation of the HF bond length to the $\rho = r - r_{eq}$ representation in terms of equilibrium displacement. We also converted from the angle θ to $y \equiv \cos\theta - 1$. We next made the expansion $V(R,r,\theta) = \Sigma_s a_s(R,\rho) y^s$. Because we have 13 data points for y for each R, r pair, we make our fit out to 12th order. Then,

$$\langle j',K|\hat{V}|j,K\rangle = \sum_s a_s(R,\rho)\langle j',K|y^s|j,K\rangle \quad \text{(A2)}$$

and so,

$$\langle k'|\langle j',K|\hat{V}|j,K\rangle|k\rangle = \sum_s \langle k'|\hat{a}_s(R,\rho)|k\rangle\langle j',K|y^s|j,K\rangle \quad \text{(A3)}$$

The evaluation of $\langle j',K|y^s|j,K\rangle$ is performed analytically (with some help from MATHEMATICA). The evaluation of $\langle k'|\hat{a}_s(R,\rho)|k\rangle$ is done numerically, using linear interpolation on $a_s(R,\rho)$ in ρ. Though we could only perform the integration over a finite ρ range for which potential data was available, we presume that the wave functions decay sufficiently rapidly outside this range that such an integration yields accurate results.

A.3. The Outgoing States. As described in section 2.3, the outgoing wave at a given energy E, corresponding to product HF in the state $|v,j,K\rangle$, is determined by averaging the Hamiltonian over the state $|v,j,K\rangle$ of interest. This gives rise to a one-dimensional Hamiltonian, given by

$$\hat{H}_R = \frac{-\hbar^2}{2\mu_R}\frac{d^2}{dR^2} + V_{vj}(R) + E_{vj} \quad \text{(A4)}$$

where $V_{vj}(R) \equiv \langle v,j,K|\hat{V}|v,j,K\rangle$. To obtain a solution $f(R)$ of energy E, we numerically integrate the following pairs of equations:

$$\frac{df}{dR} = g \quad \text{(A5)}$$

$$\frac{dg}{dR} = -\frac{2\mu_R}{\hbar^2}(E - E_{vj} - V_{vj}(R))f \quad \text{(A6)}$$

The only issue here is obtaining a set of initial conditions. The potential data only goes from some $R_{min} > 0$ to some R_{max}, so we only find the outgoing waves over this range. For simplicity, set $R \in [0, R_{min}]$, with the stipulation that f must vanish at $R = 0$. The vanishing of f at $R = 0$ is accomplished by assuming a hard wall at $R = 0$ (the difference is negligible if R is simply allowed to go to $-\infty$ and $V_{vj}(R) = V_{vj}(R_{min})$ for $\in (-\infty, R_{min}]$). The initial conditions are obtained by solving for f in the range $[0, R_{min}]$. Setting $f(R_{min}) = 1$, combined with the requirement that $f(0) = 0$, is sufficient to determine $g(R_{min}) = f'(R_{min})$.

After we obtain the solution to our system of ODE's, we need to normalize the wave function so that the outgoing states have the $\delta(E - E')$ normalization convention. This requires that the wave function have an oscillation amplitude of $(2\mu_R/\pi^2\hbar^2 (E-E_{vj}))^{1/4}$ in the large R limit.

References and Notes

(1) Buchachenko, A. A.; Stepanov, N. F.; Grigorenko, B. L.; Nemukhin, A. V. *J. Chem. Phys.* **1999**, *111*, 2470.
(2) Ewing, G. E. *J. Chem. Phys.* **1979**, *71*, 3143.
(3) Chuang, C. C.; Tsang, S. N.; Klemperer, W.; Chang, H. C. *J. Chem. Phys.* **1998**, *109*, 8836.
(4) Chuang, C. C.; Tsang, S. N.; Klemperer, W.; Chang, H. C. *J. Chem. Phys.* **1998**, *109*, 484.
(5) Hutson, J. M. *J. Chem. Phys.* **1983**, *81*, 2357.
(6) Oudejans, L.; Nauta, K.; Miller, R. E. *J. Chem. Phys.* **1996**, *105*, 10410.
(7) Halberstadt, N.; Brechignac, P.; Beswick, J. A.; Shapiro, M. *J. Chem. Phys.* **1986**, *84*, 170.
(8) Chuang, C. C.; Klemperer, W. *J. Chem. Phys.* **2000**, *113*, 4116.
(9) Miller, R. E. In *Structure and Dynamics of Weakly Bound Molecular Complexes*; Weber, A., Ed.; Reidel: Dordrecht, The Netherlands, 1987; p 131.
(10) Block, P. A.; Miller, R. E. *Chem. Phys. Lett.* **1994**, *226*, 317.
(11) Hutson, J. M. *J. Chem. Phys.* **1992**, *96*, 6752.
(12) Woon, D. E.; Dunning, T. H., Jr. *J. Chem. Phys.* **1993**, *98*, 1358.
(13) Dunning, T. H., Jr. *J. Chem. Phys.* **1989**, *90*, 1007.
(14) Kendall, R. A.; Dunning, T. H., Jr.; Harrison, R. J. *J. Chem. Phys.* **1992**, *96*, 6796.
(15) Chuang, C. C.; Higgins, K. J.; Fu, H. C.; Klemperer, W. *J. Chem. Phys.* **2000**, *112*, 7022.
(16) Segev, B.; Heller, E. J. *J. Chem. Phys.* **2000**, *112*, 4004.
(17) Dunham, J. L. *Phys. Rev.* **1932**, *41*, 713.